Published in final edited form as:
Dev Dyn. 2010 November ; 239(11): 2837–2850. doi:10.1002/dvdy.22415.

Mouse *Rad9b* is essential for embryonic development and promotes resistance to DNA damage

Corinne Leloup[1], **Kevin M. Hopkins**[1], **Xiangyuan Wang**[2], **Aiping Zhu**[1], **Debra J. Wolgemuth**[2,3,4], and **Howard B. Lieberman**[1,5,*]

[1]Center for Radiological Research, College of Physicians and Surgeons, Columbia University, New York, New York

[2]Department of Genetics and Development, Columbia University Medical Center, New York, New York

[3]Department of Obstetrics and Gynecology, Columbia University Medical Center, New York, New York

[4]The Institute of Human Nutrition, Columbia University Medical Center, New York, New York

[5]Department of Environmental Health Sciences, Mailman School of Public Health, Columbia University, New York, New York

Abstract

RAD9 participates in promoting resistance to DNA damage, cell cycle checkpoint control, DNA repair, apoptosis, embryogenesis, and regulation of transcription. A paralogue of *RAD9* (named *RAD9B*) has been identified. To define the function of mouse *Rad9b* (*Mrad9b*), embryonic stem (ES) cells with a targeted gene deletion were constructed and used to generate *Mrad9b* mutant mice. *Mrad9b*$^{-/-}$ embryos are resorbed after E7.5 while some of the heterozygotes die between E12.5 and a few days after birth. *Mrad9b* is expressed in embryonic brain and *Mrad9b*$^{+/-}$ embryos exhibit abnormal neural tube closure. *Mrad9b*$^{-/-}$ mouse embryonic fibroblasts are not viable. *Mrad9b*$^{-/-}$ ES cells are more sensitive to gamma rays and mitomycin C than *Mrad9b*$^{+/+}$ controls, but show normal gamma-ray-induced G2/M checkpoint control. There is no evidence of spontaneous genomic instability in *Mrad9b*$^{-/-}$ cells. Our findings thus indicate that *Mrad9b* is essential for embryonic development and mediates resistance to certain DNA damaging agents.

Keywords

Mrad9b; *Mrad9*; embryonic development; DNA damage sensitivity; cell cycle

INTRODUCTION

The maintenance of chromosome integrity is critical for DNA replication, cell division and embryogenesis. The byproducts of certain metabolic reactions and environmental agents can cause DNA damage and threaten this integrity. If not repaired properly, the damage can interfere with replication or transcription, and possibly lead to mutation, oncogenic transformation or death (Hanawalt and Spivak, 2008; Loeb and Harris, 2008). The cellular response to DNA damage consists of DNA repair, a transient delay in cell cycle progression called cell cycle checkpoint control, and apoptosis (Pietenpol and Stewart, 2002; Niida and

[*]**Corresponding author**. Center for Radiological Research, College of Physicians and Surgeons, Columbia University, 630 W. 168th St., New York, NY 10032, USA. Phone: (212) 305-9241. Fax: (212) 305-3229. lieberman@cancercenter.columbia.edu.

Nakanishi, 2006). Many genes involved in the DNA damage response are embryonic lethal, at least in the mouse, and/or promote tumorigenicity when null (Friedberg and Meira, 2006).

RAD9 is a multifunctional gene that plays a crucial role in cell cycle checkpoint control, DNA repair and apoptosis (Lieberman, 2006). It can also regulate the transcription of downstream target genes (Yin et al., 2004), and serve as an oncogene (Zhu et al., 2008) or tumor suppressor (Hu et al., 2008). RAD9, as a subunit of the RAD9-HUS1-RAD1 (9-1-1) complex, binds to damaged DNA, and activates a cellular response that leads to stabilization of the replication fork (Lieberman, 2006). Deletion of both *Mrad9* alleles is lethal in mice, while heterozygous *Mrad9*$^{+/-}$ mice are fully viable (Hopkins et al., 2004). Paralogues of mouse and human *RAD9*, called *Mrad9b* and *HRAD9B* respectively, have also been identified. HRAD9B protein can co-immunoprecipitate with HRAD9, as well as with other checkpoint control proteins including HRAD1, HRAD17, HHUS1 and HHUS1B (Dufault et al., 2003; Hopkins et al., 2003). It is therefore likely that *RAD9B* plays a role in some aspect of DNA repair and/or cell cycle checkpoint control. In the adult, both mouse and human *RAD9B* are predominantly expressed in testis while *RAD9* is detected in most if not all organs, suggesting that *RAD9B* could play a role in the male germ cell lineage. Furthermore, *HRAD9B* expression is reduced in testicular tumors, especially seminomas, suggesting that it functions as a tumor suppressor (Hopkins et al., 2003).

In order to characterize the function of *Mrad9b* in more detail, we used targeted recombination to generate a gene deletion in ES cells and mice. Mouse embryos null for *Mrad9b* do not survive beyond E8.5, demonstrating that *Mrad9b* is essential for early embryonic development. Some *Mrad9b*$^{+/-}$ embryos display retarded growth while others undergo prenatal or perinatal death. At E7.5, *Mrad9b* mRNA is detected in embryonic tissues. At E8.5 and E9.5, *Mrad9b* is expressed most abundantly in the brain. To begin to understand the role of *Mrad9b* in maintaining DNA integrity, homozygous mutant ES cells were examined for their responses to several types of DNA damaging agents. There was an enhanced sensitivity to gamma rays and mitomycin C, but not to hydroxyurea, cisplatin and ethyl methanesulfonate (EMS). Cell cycle distribution is normal in *Mrad9b*$^{-/-}$ ES cells not exposed to DNA damaging agents, and gamma rays can induce normal cell cycle checkpoint control in the mutant population. Furthermore, *Mrad9b*$^{-/-}$ ES cells do not demonstrate spontaneous chromosomal instability or point mutations, as is observed for *Mrad9*$^{-/-}$ cells. *Mrad9b*$^{-/-}$ mouse embryonic fibroblasts (MEFs) were not viable, but *Mrad9b*$^{+/-}$ MEFs divided as well as the WT control population. Therefore, we demonstrate that, as for *Mrad9*, *Mrad9b* is essential for proper embryonic development, as well as MEF viability. However, *Mrad9* and *Mrad9b* differ with respect to when in embryogenesis their functions are critical. Furthermore, *Mrad9b* but not *Mrad9* heterozygosity can affect embryonic viability. In addition, *Mrad9* and *Mrad9b* confer resistance to an overlapping but not identical array of DNA damaging agents.

RESULTS

Generation of *Mrad9b*$^{-/-}$ mouse ES cells

In order to characterize *Mrad9b* function, the gene was partially deleted in mouse embryonic stem (ES) cells using the targeting strategy illustrated in Fig. 1A. To generate a null mutation, the first two exons and first intron of the gene were deleted as well as 500 bp upstream of the start codon. Transfected cells were first challenged by 150 µg/ml G418. Four clones out of 130 examined by Southern blotting and PCR were heterozygous for the locus of interest, and two of them were used for further investigation. The heterozygous cells were then challenged with 800 µg/ml G418 to select for *Mrad9b* homozygous mutants (Joyner, 2000). One clone out of 69 surviving this procedure was homozygous for the *Mrad9b* deletion. Two rounds of selection with 150 µg/ml G418 were then performed to ensure the purity of the cell line. Fig. 1B shows Southern blot analysis of *Mrad9b*$^{+/+}$ ES cells, a *Mrad9b*$^{+/-}$ clone and the *Mrad9b*$^{-/-}$ clone. In the heterozygous cell population, both WT and mutant alleles are present while in the homozygous mutant, only the mutant allele is detected.

Mrad9b expression in the ES cells was determined by northern blot analysis (Fig. 1C). The most intense band in the *Mrad9b*$^{+/+}$ sample is the size predicted for the *Mrad9b* mRNA, based on previously isolated cDNAs (1.9 kb; Hopkins et al., 2003). This band is detected at a lower intensity in the heterozygous cells compared to the WT cells and is not present in *Mrad9b* null cells. We also observed additional bands in all the samples, but at sizes that do not correspond to the spliced *Mrad9b* message. We have not determined the origin of these extra bands. However, the upper most band found in *Mrad9b*$^{+/-}$ and *Mrad9b*$^{-/-}$ samples could be a read-through fusion transcript originating from a gene upstream of *Mrad9b* and containing the partially deleted *Mrad9b*. The other bands might represent alternatively spliced *Mrad9b* messages. *Mrad9b* expression levels were confirmed by semi-quantitative RT-PCR using primers corresponding to the first and second *Mrad9b* exons, and *beta-actin* expression as an internal standard (data not shown). These results indicate that *Mrad9b* expression was about half in each of the two heterozygous clones compared to WT cells (44% for clone 341 and 38% for clone 350), as predicted.

Mrad9b is essential for early embryonic development

Mrad9b$^{+/-}$ mice were obtained by injection of *Mrad9b*$^{+/-}$ ES cells into blastocysts and transfer to foster mothers as described in the Experimental Procedures section. The PCR strategy used to genotype mice is illustrated in the gel in Fig. 1D. *Mrad9b*$^{+/-}$ intercrosses yielded no homozygous mutant offspring after 17 rounds of matings. Pups that were born consisted of 43 wild type and 38 heterozygotes (Table 1). This corresponds to a ratio of 1:0.88:0 for wild type:heterozygote:mutant, which is not consistent with Mendelian predictions (1:2:1). These results indicate that homozygotes are not viable and that some heterozygotes die before the time of genotyping (one month after birth), thus during gestation or perinatally.

In order to determine the developmental stage at which *Mrad9b* null mutant and heterozygous embryos die, timed matings were set up between *Mrad9b*$^{+/-}$ male and female mice. Embryos were collected at selected days of gestational development, beginning at embryonic day E7.5 (Table 1). Starting from E8.5, homozygous mutant embryos were resorbed. E11.5 or older *Mrad9b* null embryos were not obtained at all, indicating that at least one *Mrad9b* gene copy is essential for viability after E7.5. For E12.5 and younger embryos, the ratio of wild type:heterozygote followed Mendelian predictions (1:2), but for E14.5 embryos, the ratio was 1:1.2. The lower than expected number of heterozygous embryos suggests that some of these animals die before birth. We found that of the 5 pups that died right after birth and were analyzed, all were heterozygous for the *Mrad9b* deletion mutation. These results indicate that heterozygotes die from E12.5 to one or two days after birth. While it is possible that heterozygous *Mrad9b* mice die beyond this time point, we have not observed this to date.

Inspection of embryonic morphology at E7.5 revealed no obvious differences among wild-type, heterozygous and mutant animals (data not shown). At E8.5, several *Mrad9b* heterozygous embryos were smaller than their WT littermates (data not shown), and one was resorbed (Table 1). In order to determine whether this is due to a developmental defect or developmental delay, somites were counted in E8.5 embryos originating from 4 litters. Close to the expected number of somites at this stage of development, 7–8 (Kaufman, 1995), was observed in WT embryos (Table 2). If heterozygotes were uniformly developmentally delayed, the number of somites would be predicted to be shifted towards lower numbers relative to WT. However, heterozygotes displayed high heterogeneity in the numbers of somites, ranging from 0 to 11 (Table 2). This difference in the distribution of somite numbers for *Mrad9b*$^{+/+}$ and *Mrad9b*$^{+/-}$ embryos is significant as calculated by the Levene test of homogeneity of variance with the SPSS program (p=0.01). These results suggest a developmental defect in some of the *Mrad9b*$^{+/-}$ embryos at E8.5 rather than a uniform developmental delay. Only two E8.5 homozygotes were found in this group of E8.5 embryos. One had 7 somites, which is in the expected range; the other was too small to permit scoring.

There was further morphological heterogeneity among the *Mrad9b*$^{+/-}$ embryos at later stages of development. At E9.5, 2 out of 21 *Mrad9b*$^{+/-}$ embryos exhibited incomplete neural tube closure, while at E10.5, 5 out of 16 heterozygous embryos demonstrated this defect. Fig. 2 shows external and histological morphologies of E10.5 embryos originating from the same litter. Fig. 2a and 2b show two WT embryos that differ only by size. In Fig. 2c, a thin section of the same embryo as in Fig. 2a is shown after hematoxylin/eosin (H&E) staining. Fig. 2d shows a morphologically normal *Mrad9b* heterozygous embryo, while Fig. 2e shows a heterozygous embryo with a defect in neural tube closure. This defect is also observable in Fig. 2f, where a histological section of the latter embryo is presented. Examples of a non-viable (Fig. 2g, i) and a resorbed (Fig. 2h) homozygous null embryo are also presented.

Overall, these results demonstrate that *Mrad9b* is essential for embryonic development. They also indicate that *Mrad9b* likely plays an important role in brain development.

***Mrad9b* is expressed in embryonic neural tissues**

To more fully explore a role for *Mrad9b* in brain development, we assessed its expression by whole mount *in situ* hybridization of WT embryos using full length antisense (Fig. 3a, c, e) and sense probes (Fig. 3b, d, f). At E7.5, *Mrad9b* is expressed mainly in embryonic tissues, as opposed to extra-embryonic tissues (Fig. 3a), and particularly in the brain at E8.5 and E9.5 (Fig. 3c, e). Positive staining of the otocyst at E9.5 is not specific because a positive signal was also obtained with the sense probe (Fig. 3f). These results provide additional evidence that *Mrad9b* is important for brain formation.

Reduced cellular proliferation in *Mrad9b*$^{-/-}$ embryos

To begin to determine the molecular mechanisms contributing to the embryonic lethality and defects in brain development in *Mrad9b*$^{+/-}$ and *Mrad9b*$^{-/-}$ embryos, E9.5 embryos were examined for cellular proliferation using a 5-bromo-2'-deoxyuridine (BrdU) incorporation assay. Representative sections of the tissues analyzed are presented in Fig. 4A. Both the WT and heterozygous embryos examined were of normal size, while the *Mrad9b*$^{-/-}$ embryo was much smaller and underdeveloped. It was possible to recognize the head from the posterior part but internal organs could not be identified. In the mesenchyme of the forebrain, there were 54.1±5.1% BrdU positive cells in the WT embryo, 58.0±9.7 % in the heterozygote and 35.2% in the mutant. In the neuroepithelium of the forebrain, there were 32.6±15.7% BrdU positive cells in the WT embryo, 64.3±3.3% in the heterozygote and 11.9% in the mutant. In the somites, there were 57.9±8.8% in the WT, 59.8±3.4% in the heterozygote and 22.3% in the mutant. In every tissue, the percentage of proliferating cells is much lower in the homozygous mutant than in the WT and heterozygote embryos. Between 2 and 4 sections were analyzed each for the WT and the *Mrad9b* heterozygous embryos. Only one *Mrad9b*$^{-/-}$ embryo section could be analyzed because of the small size and limited number of samples. Results are presented as average ± standard deviation. Defects in cellular proliferation could thus be involved with the death of the embryos. Alternatively, it is also possible that the homozygous embryo is close to death and all its physiological functions have already shut down. The low percentage of dividing cells in the neuroepithelium of the

Mrad9b$^{+/+}$ embryo relative to that of the *Mrad9b*$^{+/−}$ embryo is unexpected. Additional experiments are needed to define the biological significance and underlying mechanisms.

The same E9.5 embryos were also examined for apoptotic cell death by TUNEL staining (Fig. 4B). Apoptotic cells were detected only sporadically throughout the embryos regardless of genotype. Overall, there is a very similar distribution of apoptotic cells for the *Mrad9b*$^{+/+}$, *Mrad9b*$^{+/−}$ and *Mrad9b*$^{−/−}$ embryos. Therefore, aberrant apoptosis is not likely contributing to the demise of the mutant embryos.

Mrad9b is required for viability of MEFs

In order to determine whether *Mrad9b* is essential for MEF viability, we attempted to generate these cells from E8.5 *Mrad9*$^{+/+}$, *Mrad9b*$^{+/−}$ and *Mrad9b*$^{−/−}$ embryos. Two WT and four *Mrad9b*$^{+/−}$ MEF cultures were obtained and could be passaged at least six times. The *Mrad9b*$^{+/−}$ MEFs did not show any obvious difference in morphology or growth rate relative to the WT controls. The *Mrad9b*$^{+/+}$ and *Mrad9b*$^{+/−}$ MEFs were passaged and reached confluency at the same time. After one replating, the *Mrad9b*$^{−/−}$ MEFs (from two different embryos) stopped growing and started dying. Therefore, we conclude that Mrad9b protein is essential for viability of MEFs but not for ES cells.

In order to determine whether size differences between *Mrad9b*$^{+/−}$ embryos could be explained by a difference in the rate of cell division, we calculated population doubling time in MEFs derived from E13.5 embryos. Two WT and six *Mrad9b*$^{+/−}$ embryos were obtained from a single litter and used for deriving MEFs. Out of the six *Mrad9b*$^{+/−}$ embryos, three were of similar size and gross morphology compared to the WT embryos, two were smaller and one had a defect in neural tube closure. There was no significant difference in doubling time between *Mrad9b*$^{+/+}$ MEFs (23.1±4.2 hr, and 17.7±1.3 hr) and *Mrad9b*$^{+/−}$ MEFs derived from embryos displaying the various phenotypes (“WT-like” phenotype: 21.5±6.4 hr; 17.5±1.6 hr and 22.7±5.7 hr; “smaller than WT” phenotype: 31.6±9.2 hr and 20.8±1.6 hr; “with defect in neural tube closure” phenotype: 23.1±4.3 hr). Numbers represent the average doubling times in hours for 2 or 3 independent repeats ± standard deviation. *Mrad9b* expression was monitored during exponential growth and when cells reached confluency by semi-quantitative PCR using *beta-actin* as an internal standard. *Mrad9b* RNA abundance in *Mrad9b*$^{+/−}$ MEFs was approximately one third to one half the level observed in *Mrad9b*$^{+/+}$ MEFs, regardless of the corresponding *Mrad9b*$^{+/−}$ embryonic phenotype (data not shown).

Mrad9b$^{−/−}$ ES cells are hypersensitive to gamma rays and mitomycin C

Since *Mrad9* promotes cell survival after exposure to certain DNA damaging agents (Hopkins et al., 2004), we tested whether the related *Mrad9b* gene has a similar function. *Mrad9b*$^{+/+}$ and *Mrad9b*$^{−/−}$ ES cells were plated at low density and treated with various DNA damaging agents. Eight days later, colonies originating from surviving cells were counted. As shown respectively in Fig. 5A and 5B, *Mrad9b*$^{−/−}$ cells are very sensitive to gamma rays and mitomycin C when compared with the *Mrad9b*$^{+/+}$ control. The knockout ES cells were not relatively more sensitive than controls to hydroxyurea (Fig. 5C), cisplatin (Fig. 5D) and EMS (Fig. 5E). Therefore, *Mrad9b* confers upon cells sensitivity to a select array of DNA damaging agents.

The sensitivity of two independent *Mrad9b*$^{+/−}$ ES cell populations to gamma rays (Fig. 5A) and mitomycin C (Fig. 5B) was examined. Clone 341 consistently demonstrated essentially WT levels of resistance to both of these agents, whereas clone 350 showed sensitivity profiles similar to *Mrad9b*$^{−/−}$ cells. This variation of heterozygote sensitivity to DNA damaging agents is interesting in that it is consistent with the variability found for the *Mrad9b*$^{+/−}$ mice with respect to abnormal embryonic development and viability.

The ability of ectopic expression of the *Mrad9b* cDNA to restore high levels of resistance of *Mrad9b*$^{-/-}$ ES cells to gamma rays and mitomycin C was examined. Expression plasmid pcDNA3.1/Hygro-Mrad9b was transfected into the mutant ES cells, which were then tested for sensitivity to these agents. Interestingly, only two of four stable transfectants expressing *Mrad9b* and tested demonstrated wild-type levels of resistance to both gamma rays and mitomycin C (data not shown). These results indicate that the sensitivity of *Mrad9b*$^{-/-}$ cells to these agents is due to loss of function of that gene. In addition, the lack of complementation in all transfectants examined is consistent with the variability of heterozygote ES cell sensitivity to DNA damage and *Mrad9b*$^{+/-}$ embryo abnormalities observed.

Mrad9b is not involved in G2/M cell cycle checkpoint control

Mrad9-deficient mouse ES cells are unable to maintain ionizing radiation-induced G2 cell cycle phase delay. We therefore examined a potential role for *Mrad9b* in cell cycle regulation. The doubling time for *Mrad9b* null ES cells and the WT control is similar, 12.1± 0.1 h versus 12.6 ± 0.8 h, respectively. We also examined the cell cycle phase profiles for *Mrad9b*$^{+/+}$ and *Mrad9b*$^{-/-}$ populations unirradiated or exposed to 8 Gy of gamma rays. The results are presented in Fig. 6 and Table 3. Asynchronously growing, unirradiated *Mrad9b*$^{+/+}$ ES cells are distributed in cell cycle phases as follows: G1 (35.1%), S (28.5%) and G2/M (36.4%). Exposure to a dose of 8 Gy of gamma rays induced a transient G2/M delay for those cells. The percentage of WT cells in G2/M rises to a maximum of 82.4% at 8 hrs after irradiation. About 12 hrs post-irradiation the cells start to resume cycling. Untreated *Mrad9b*$^{-/-}$ cells had a cell cycle distribution similar to the wild type control, 30.8% in G1, 32.5% in S, and 36.7% in G2/M. Much like the wild type, the number of mutant cells in G2/M increased after irradiation until it reached a peak of 80%, 8–12 hrs after irradiation. Subsequently, the mutant cells resumed cycling. Both *Mrad9b*$^{+/+}$ and *Mrad9b*$^{-/-}$ populations had an increased number of cells in S phase at 4 hrs post-irradiation. Compared to wild-type cells, *Mrad9b*$^{-/-}$ cells did not display any irregularity in radiation-induced cell cycle delay. Furthermore, both populations continued cycling normally about the same time after irradiation, unless they were blocked in G2 by treatment with nocodazole.

Mrad9b is not essential for maintaining genomic integrity

To establish whether *Mrad9b* is important for maintaining genomic integrity, the frequencies of sister chromatid exchange (SCE) and micronuclei formation were determined in ES cells not exposed to exogenous DNA damaging agents. As indicated in Fig. 7A, there is no difference between *Mrad9b*$^{+/+}$ and *Mrad9b*$^{-/-}$ cell lines with respect to spontaneous SCE frequency. Fig. 7B shows that differences in the number of micronuclei in binucleated *Mrad9b*$^{+/+}$ and *Mrad9b*$^{-/-}$ cells were not statistically significant. *Mrad9b*$^{+/+}$ cells had 4.4±1.3 micronuclei per 100 cells examined, whereas the *Mrad9b*$^{-/-}$ population demonstrated a frequency of 3.5±0.7 micronuclei per 100 cells. In addition, no *HPRT* mutations were detected in 10^7 *Mrad9b*$^{+/+}$ and *Mrad9b*$^{-/-}$ cells using an assay described previously (Hopkins et al., 2004), and thus indicating the absence of a high spontaneous frequency of gene point, deletion or other alterations. Moreover, preliminary karyotype analysis of M-FISH stained chromosomes did not reveal major spontaneous chromosomal aberrations in either cell population (data not shown). Therefore, using several different assays, no evidence for a role of *Mrad9b* in maintaining genomic integrity was observed.

DISCUSSION

Properties of mouse embryonic stem cells and fibroblasts with targeted deletion of *Mrad9b*

Mouse ES cells bearing a targeted deletion of *Mrad9* demonstrate genomic instability, sensitivity to a variety of DNA damaging agents, and difficulty maintaining gamma-ray-induced delay in the G2 phase of the cell cycle, relative to controls (Hopkins et al., 2004). *RAD9B* was identified as a *RAD9* paralogue, thus revealing the existence of a gene family (Hopkins et al., 2003). In order to define the function of *Mrad9b* in mice, we constructed mouse ES cells and mice with a targeted deletion of the gene. Heterozygous and homozygous *Mrad9b* null ES cells were viable, and had doubling times similar to that observed for the WT control. Therefore, *Mrad9b* is not essential for viability of ES cells. However, it is essential for MEFs since *Mrad9b*$^{-/-}$ viable cells of this type could not be obtained. This is somewhat surprising because ES cells are generally more sensitive to genotoxic stress than MEFs (de Waard et al., 2008), and it would thus be expected that the latter cells would have less of a requirement for a DNA damage response gene like *Mrad9b*, even to handle spontaneous damage. There are several studies showing that it is possible to grow viable MEFs lacking DNA damage response genes, even when loss of the same genes leads to embryonic death. For example, it is possible to construct MEFs with deletion of the following genes: *Pol-beta*, which participates in base excision repair (BER) (Sobol et al., 1996), *Ddb1*, *Hr23B* and *Xpa*, which mediate nucleotide excision repair (NER) (Ng et al., 2002; Cang et al., 2006; de Waard et al., 2008), *Brca1* and *Xrcc2*, involved in homologous recombination repair (HRR) (Zhong et al., 2002; Orii et al., 2006), and the checkpoint control genes *Rb* and *p53* (Herrera et al., 1996; Menon et al., 2003). MEFs deleted for *Lig4*, a nonhomologous end joining (NHEJ) gene, can grow but have a lower proliferative capacity than WT MEFs (Frank et al., 1998). *Mrad9*$^{-/-}$ and *Hus1*$^{-/-}$ MEFs, in contrast to ES cells with the same genotypes, are not viable (Weiss et al., 2000; Hopkins et al., 2004). Perhaps functions of *Mrad9* and *Mrad9b* unrelated to DNA damage repair are required for MEF viability, but further study is needed to resolve this issue.

Mrad9b is essential for early embryonic development

Resorption of *Mrad9b*$^{-/-}$ mouse embryos can occur at slightly different stages of development and is first observed starting at E8.5. This pattern of embryonic lethality occurs at about the same developmental stages seen in deletions of two of the genes involved in HRR. *Brca1*$^{-/-}$ embryos die between E5.5 and E10.5 (Gowen et al., 1996; Hakem et al., 1996; Liu et al., 1996; Ludwig et al., 1997), and *Brca2*$^{-/-}$ embryos die between E6.5 and E9.5 (Ludwig et al., 1997; Sharan et al., 1997; Suzuki et al., 1997). Lack of *Xrcc1* (a gene involved in BER) also results in embryonic lethality around E7.5-E8.5 (Tebbs et al., 1999). *Mrad9*$^{-/-}$ embryos die between E9.5 and E12.5 (Hopkins et al., 2004), indicating that *Mrad9b* function is essential for embryogenesis at an earlier stage than its paralogue.

The failure of embryos to survive in the absence of *Mrad9b* might be due at least in part to decreased cellular proliferation rather than increased apoptosis. Similarly, in *Brca1*$^{-/-}$ (when either exon 11 or both exons 1 and 2 were deleted) as well as *Brca2*$^{-/-}$ embryos, the rate of cellular proliferation is reduced while the frequency of apoptosis is normal (Hakem et al., 1996; Liu et al., 1996; Suzuki et al., 1997). Interestingly, despite the known role for *p53* in apoptosis, there is also no difference in the frequency of this process when brain specimens of *p53*$^{-/-}$ and *p53*$^{+/+}$ mouse embryos are compared (Sah et al., 1995).

Characteristics of *Mrad9b* heterozygous mutant mice

Several but not all *Mrad9b*$^{+/-}$ embryos display gross morphological abnormalities and stunted growth. In some cases, heterozygotes demonstrated an open brain phenotype, probably caused by a defect in neural tube closure. More than 50 genes with various molecular functions are involved in neural tube closure (Harris and Juriloff, 1999), including genes that contribute to the DNA damage response. For example, mouse embryos with an exon 11 deletion of *Brca1* fail to close their neural tubes at E9.5–10.5 (Gowen et al., 1996). A small fraction of *p53*$^{+/-}$ and *p53*$^{-/-}$ embryos also display a defect in neural tube closure, which later (around E13.5) develops as exencephaly (Sah et al., 1995). Homozygous deletion of checkpoint control genes *Hus1* and *Rad17* in mouse embryos leads to neural tube defects at E9.5 and E11.5, respectively (Weiss et al., 2000; Budzowska et al., 2004). Failure of neural tube closure might be a byproduct of a general disturbance in development, but the fact that *Mrad9b* is expressed in the embryonic brain at E8.5–9.5 supports the hypothesis that *Mrad9b* is specifically involved in brain formation. More experiments are needed to unravel its exact role, but *Mrad9b* seems to be involved specifically in the development of the anterior part of the nervous system because a defect in the caudal part of the neural tube has not been observed. Defects in neural tube closure are not detected in *Mrad9b* null mutants, as they never reach this stage of development.

The subset of *Mrad9b*$^{+/-}$ mouse pups that survive appear normal and are clearly fertile. However, brain morphology or neural function were not examined in adult mice. Therefore, some of these adult heterozygous animals might have subtle brain abnormalities that are compatible with viability.

In the adult, *Mrad9b* is expressed mainly in the testis (Hopkins et al., 2003). It seems that *Mrad9b* switches from having a function in general development and/or in brain development in the early embryo to having another function in the adult testis. Alternatively, *Mrad9b* might have one biochemical activity that manifests differently in the different tissue environments. There is precedent for this in rats, as some genes involved in embryonic neuronal development, such as *chemokine receptor 4* (*Cxcr4*), *glypican 4* (*Gpc4*), *microtubule-associated protein 1b* (*Map1b*) and *cyclin-dependent kinase 5* (*Cdk-5*) eventually become expressed in cells undergoing spermatogenesis (Johnston et al., 2008).

ES cells null for *Mrad9b* are sensitive to certain DNA damaging agents

Mrad9b$^{-/-}$ ES cells are sensitive to ionizing radiation, which induces mainly DNA double strand breaks (DSBs), single strand breaks (SSBs) and base damage (Jeggo and Lobrich, 2006). DSBs are repaired by NHEJ and HRR (Jeggo and Lobrich, 2006). SSBs are repaired either by simple ligation or by BER (Dianov and Parsons, 2007), and base damage is repaired by the latter (Robertson et al., 2009). ES cells in which most of the HRR genes (*Brca2*, *Chk1*, *Mre11*, *Nbs1*, *Rad50* and *Rad51*) are individually mutated are not viable (Lim and Hasty, 1996; Sharan et al., 1997; Xiao and Weaver, 1997; Luo et al., 1999; Liu et al., 2000; Zhu et al., 2001) but E3.5 mouse blastocysts mutant for *Brca2*, *Rad50* and *Rad51* (Lim and Hasty, 1996; Sharan et al., 1997; Luo et al., 1999) are more sensitive to ionizing radiation, relative to WT controls, and *Chk1* conditional knockout mouse ES cells are defective for G2/M checkpoint control induced after exposure to ionizing radiation (Liu et al., 2000). It is possible, however, to construct ES cells that are deficient for NHEJ genes. For example *Ku70*$^{-/-}$, *Ku80*$^{-/-}$, *Xlf* $^{-/-}$and *Xrcc4*$^{-/-}$ mouse ES cells (Nussenzweig et al., 1996; Gu et al., 1997; Gao et al., 1998; Zha et al., 2007) are viable but all are more sensitive to ionizing radiation relative to WT ES cells. HRAD9 interacts with HRAD51, a protein that plays a major role in homologous recombination (HR), and cells expressing siRNA targeting HRAD9 have decreased HR activity, strongly suggesting that HRAD9 is involved in this repair process (Pandita et al., 2006). Further, *HRAD9* is not involved in NHEJ, as demonstrated by a DNA end-joining assay (Pandita et al., 2006). HRAD9, either by itself or as a complex with HRAD1 and HHUS1, interacts with and stimulates proteins involved in the BER pathway (Helt et al., 2005; Lieberman, 2006). As a *RAD9* paralogue, *RAD9B* could also be involved in BER. However, *Mrad9b*$^{-/-}$ cells do not display increased sensitivity to

EMS, which causes DNA alkylation that serves as a substrate for BER (Sega, 1984; Robertson et al., 2009), making it less likely that *Mrad9b* functions in that DNA repair pathway.

Finally, deletion of *Mrad9b* in mouse ES cells confers sensitivity to mitomycin C. This chemical generates inter- and intrastrand DNA crosslinks as well as DNA monoadducts (Palom et al., 2002). It is somewhat unexpected that *Mrad9b*$^{-/-}$ cells are not sensitive to cisplatin because this chemical generates similar types of DNA damage (Rabik and Dolan, 2007). However the actions of these chemicals are not strictly identical. Mitomycin C targets principally the N2-position of guanine (Warren et al., 1998) while cisplatin targets mainly the N7-position of guanine (Rabik and Dolan, 2007). Interstrand crosslinks are the most toxic lesion generated by mitomycin C (Palom et al., 2002) and cisplatin toxicity seems to depend mainly on intrastrand cross links (Fuertes et al., 2003). The crosslinks generated by cisplatin are more bulky than those generated by mitomycin C (Warren et al., 1998). These differences can explain the differential cell sensitivity observed. In V79 hamster cells, cisplatin-induced crosslinks are repaired while mitomycin C-mediated crosslinks are not (Larminat et al., 1998). Interstrand crosslinks are repaired mainly via NER and homologous recombination pathways, with the creation of a DSB repair intermediate (McHugh et al., 2001). Clearly, more work is needed to define the role of *Mrad9b* in these repair processes.

Conclusion

In summary, a null deletion of the *Mrad9b* gene results in embryonic lethality between days E8.5 and E10.5 of development, which may in part be due to decreased cellular proliferation. Interestingly, heterozygosity for *Mrad9b* deletion leads to lethality in approximately one half of later-stage embryos or early postnatal pups. *Mrad9b* is expressed in the brain of mouse embryos at least at E8.5 and E9.5, and some *Mrad9b*$^{+/-}$ embryos demonstrate a failure of neural tube closure. *Mrad9b* is not essential for mouse ES cell viability but it is critical for MEFs. Although there does not appear to be a role for *Mrad9b* in maintaining genomic integrity in the absence of exogenous DNA damaging agents, it promotes cellular resistance to certain types of DNA damage. Finally, we demonstrate that *Mrad9b*$^{-/-}$ ES cells display a normal G2/M delay after gamma irradiation, which is different from *Mrad9*$^{-/-}$ mouse ES cells where the checkpoint can be initiated but not readily maintained (Hopkins et al., 2004).

EXPERIMENTAL PROCEDURES

Plasmid construction

A targeting vector was made to replace the first two exons and first intron of *Mrad9b* as well as 500 bp upstream of the start of translation, by a *loxP-neo-loxP* cassette (*NEO-loxP* in Fig. 1A) encoding neomycin phosphotransferase and capable of conferring cellular resistance to neomycin (G418). A 2.3 kb fragment ("a" in Fig. 1A) was amplified by PCR upstream of the region to be deleted using primers 5'-ACTTTGATCATAGACAGACAGTAGAGGCAG-3' and 5'-ATTATGATCACCGGACCCGGTCACGAGATC-3'. A 3.4 kb fragment ("b" in Fig. 1A) downstream of that region was amplified using primers 5'-TCACTGTCGACGCCAGGTGTGCCTCAAATCCCA-3' and 5'-TCAAC CTCGAGACAGTCCTGCCTTTGGTCCT-3'. Restriction sites were added on the 5' ends of the primers as indicated in Fig. 1A. PCR fragments "a" and "b" were subcloned separately into plasmid vector TOPO-XL (Invitrogen, CA), and DNA sequence analysis was performed to confirm their identities. Fragment "b" was cut with *Sal*I and *Xho*I from TOPO-XL, then ligated into the *Sal*I site of vector pKSloxPNT (Hanks et al., 1998). Then the "a" fragment was cut from TOPO-XL with *Bcl*I and ligated into the *Bam*HI site of the modified pKSloxPNT plasmid to create the targeting vector TK-a-loxP-NEO-loxP-b (Fig. 1A).

A vector capable of expressing *Mrad9b* was constructed. *Mrad9b* cDNA (Hopkins et al., 2003) was cut with *Eco*RV and *Xba*I from the N-terminal pFLAG-CMV vector (Sigma), and the latter restriction enzyme site on the gene-containing fragment was filled in to create a fragment with two blunt ends. This fragment was then ligated into the *Eco*RV site of pcDNA3.1/Hygro (Invitrogen) to create the expression vector pcDNA3.1/Hygro-Mrad9b.

ES cell culture, gene targeting, production of *Mrad9b*-deficient ES cells and doubling time

Mouse ES cells were grown in tissue culture dishes coated with 0.1% gelatin in Knockout™ DMEM (Gibco/Invitrogen, CA) containing 15% ES cell qualified fetal bovine serum (Gibco/Invitrogen, CA), 1x MEM non-essential amino acid solution, 2 mM L-glutamine, 100 U penicillin, 100 U streptomycin and 1×10^{-4} M β-mercaptoethanol per 500 ml DMEM. The targeting vector was purified by centrifugation on a cesium chloride gradient and linearized with *Avr*II before electroporation into 129 SvEvTac mouse ES cells, which were subsequently seeded at a density that allows for 1–20 colonies to grow per dish (~10^7 cells plated per 10 cm dish). Transformed cells that underwent homologous recombination of the target vector into the genome were selected for resistance to G418 (150 μg/ml) mediated by the neomycin resistance gene. Cells that integrated the vector in a non-homologous manner were selected against by challenging with 2 μM ganciclovir. The thymidine kinase gene sensitizes those cells to the drug. *Mrad9b*$^{+/-}$ cells identified were challenged with 800 μg/ml G418 to select for *Mrad9b* homozygous mutant derivatives (Joyner, 2000). Two rounds of selection with 150 μg/ml G418 were then performed to ensure purity of the cell line.

For the doubling time calculation, 2×10^4 ES cells were seeded in triplicate into gelatinized 6-well dishes. Cell numbers were determined every 24 hours for the duration of the experiment. Doubling time was calculated in the exponential growth phase.

Generation of mouse embryos

Mrad9$^{+/-}$ ES cells (129/SvEvTac) were injected into blastocysts from C57BL/6J mice, and the blastocysts were transferred to B6CBAF1 foster mothers according to standard procedures (Joyner, 2000). Chimeric males resulting were mated with *Mrad9b*$^{+/+}$ C57BL/6J females to mediate germline transmission of the *Mrad9b* mutant allele. Subsequent crosses involving the offspring produced *Mrad9b* heterozygous animals. These mice were intercrossed and the resulting embryos were obtained at several stages of gestation (E7.5, E8.5, E9.5, E10.5, E11.5, E12.5, E14.5). Day E0.5 was considered noon of the day when a vaginal plug was detected. All dissections were performed in 1x PBS.

Southern blotting, PCR and northern blotting assays

Cells were screened for the status of *Mrad9b* by examining the downstream 3.4 kb fragment (“b” fragment in Fig. 1A) by Southern blotting. Cells were allowed to grow in 96 well plates until reaching confluence. Genomic DNA was isolated using published protocols (Joyner, 2000). Cells were washed twice with PBS, lysed overnight at 55°C in a buffer containing 10 mM Tris-HCl pH 7.5, 10 mM EDTA, 10 mM NaCl, 1 mg/ml proteinase K and 0.5% SDS. A freshly made NaCl/ethanol mix (75 mM NaCl in absolute cold ethanol) was then added to the cells, which were incubated for at least one hour at room temperature. Precipitated DNA was washed three times with 70% ethanol and air-dried. DNA was then digested overnight by *Nde*I and *Bst*Z17I. DNA was separated on a 0.7% agarose gel, transferred to a nylon membrane, and hybridized to a 489 bp *Mrad9b* probe, which corresponds to a sequence downstream of the targeting site (see Fig. 1A and Fig. 1B). The probe had been PCR amplified from a site downstream of the 3.4 “b” fragment using mouse genomic DNA as template in conjunction with primers 5’-CTGTTGAGTGTAGTGGTGGA-3’ and 5’-GCATGTGTATGGAGGTCGAA-3’. The amplified fragment had been TA-cloned into plasmid vector pCRII (Invitrogen, Carlsbad, CA), cut with *Eco*RI, gel purified and randomly labeled with ^{32}P.

Recombination of the upstream 2.3 kb fragment (“a” fragment in Fig. 1A) was assessed in the heterozygous *Mrad9b* cell clones by PCR using sense primer 5’-GCCACAGCACCCCTGACAATTAGTGTGT-3’ (*Mrad9b* gene) and anti-sense primer 5’-GCAATCCATCTTGTTCAATGGCCGATCC-3’ (*Neo* gene). Sequence analysis was performed to confirm the identity of the cloned DNA.

Mrad9b expression was examined by northern blotting analysis. Total RNA was extracted with Trizol (Invitrogen, Carlsbad, CA) and further purified to obtain mRNA using the QIAGEN (Valencia, CA) Oligotex kit as specified by the manufacturer. mRNA was separated on a 1% agarose gel containing MOPS and formaldehyde, then transferred to a nylon membrane and hybridized to a *Mrad9b* RNA probe. *Mrad9b*-pGEMT plasmid (Joyner, 2000; Hopkins et al., 2003) was digested with *Nde*I, and T7 polymerase (Strip-EZ™ RNA from Ambion, Austin, TX) was used to synthesize ^{32}P labeled probe. Loading was monitored using a RNA probe for beta-actin (Strip-Easy, Ambion, TX).

For PCR genotyping of mice, genomic DNA was isolated from tail fragments using DirectPCR (Tail) lysis reagent (Viagen Biotech Inc., Los Angeles, CA). To genotype for assessing *Mrad9b* status, primers 5'-CTTGGGTGGAGAGGCTATTC-3' and 5’-AGGTGAGATGACAGGAGATC-3’ were used to amplify the *Neo* gene (size of fragment: 280 bp); primers 5'-GTGTGGTGAATTCCTGTCATGGTG-3' and 5’-CACTGAACAACTTAGTCATGCCTG-3’ were employed to amplify *Mrad9b* (size of fragment: 450 bp). PCR conditions were 94°C for 3 min followed by 2 cycles of 94°C for 20s, 64°C for 30s, and 72°C for 35s. The annealing temperature was then stepped down one degree each second cycle until 58°C where 25 cycles were performed. There was a final extension at 72°C for 2 min. PCR products were resolved on agarose gels.

Whole mount *in situ* hybridization

Sense and antisense RNA probes for *in situ* hybridization were transcribed from the SP6 and T7 promoters of *Mrad9b*-pGEMT plasmid (Hopkins et al., 2003) linearized with *Aat*II and *Nde*I respectively. Reactions were terminated with 0.025M EDTA and probes were purified by sodium acetate/ethanol precipitation, following the manufacturer’s suggested protocols (MAXIscript SP6/T7 kit, Ambion). Probes used for *in situ* hybridization were labeled with digoxigenin-11-UTP, using the Roche Diagnostics RNA labeling kit (Roche, Germany).

E7.5, E8.5 and E9.5 embryos were collected in 1x PBS, fixed for 2 hr in freshly prepared PFA (4% paraformaldehyde in 1x PBS) and stored in 100% methanol at −20°C. Embryos were processed for whole-mount *in situ* hybridization according to protocols from Hogan and coworkers (Hogan B., 1994). Briefly, embryos were rehydrated in PBST (1x PBS, 0.1% Tween 20), washed in RIPA buffer (150 mM NaCl, 1% Nonidet P-40, 0.5% sodium deoxycholate, 0.1% SDS, 1mM EDTA, 50 mM Tris-Cl, pH 7.6), post-fixed with PFA, and then washed with PBST. They were pre-hybridized in 50% formamide, 5x SSC, 20 mM sodium phosphate buffer, pH 7.4, 0.1% Tween 20, 100 μg/ml yeast tRNA, 100 μg/ml ssDNA at 70° C for 3 hr and hybridized overnight in the same solution plus probe in a chamber humidified with 50% formamide in water at 70° C. The embryos were then washed 3 times and treated with blocking solution (10% sheep serum plus 3% BSA in PBS) for 2 hr, and then with a 1:2000 dilution of anti-digoxygenin alkaline phosphatase-tagged antibody (Roche Diagnostic) before incubation overnight at 4° C. Samples were then washed in

TBST (150 mM NaCl, 25 mM Tris-Cl, pH 7.6, 0.1% Tween 20) at 4° C overnight with gentle rocking, followed by washing 3 times in NTMT (100 mM NaCl, 100 mM Tris-HCl, pH 9.5, 50 mM $MgCl_2$, 0.1% Tween-20). The washing solution was removed and the reaction mix (125 µg/ml 5-bromo-4-chloro-3-indolyl phosphate (BCIP) and 259 µg/ml nitro blue tetrazolium NBT in NTMT) was added and allowed to develop overnight at 4°C. Following staining, embryos were post-fixed in PFA, washed in PBS and photographed under a Wild Heerbrugg photomicroscope with dark field.

Morphology, histology, cellular proliferation and apoptosis in mouse embryos

For gross morphological analyses, whole embryos were rinsed with 1x PBS. For histological analysis, sections were stained with H&E.

For apoptosis and BrdU incorporation assays, embryos produced from a timed *Mrad9b* heterozygote intercross were isolated at E9.5. Samples were fixed and embedded in paraffin as described previously (Chapman and Wolgemuth, 1994). Sections (5 µm thick) were cut.

To analyze BrdU incorporation as a measure of DNA replication, BrdU was injected intraperitoneally into females carrying E9.5 day embryos at 100 µg per gram of body weight (Weiss et al., 2000). One hr after BrdU injection, embryos were isolated, fixed, and sectioned as described above. BrdU staining was performed with a biotinylated mouse anti-BrdU antibody using a BrdU staining kit (Oncogene Inc.), as per the manufacturer. DAB was used as the peroxidase substrate and counterstaining was performed with hematoxylin. Dividing cells were counted in the mesenchyme and the neuroepithelium of the forebrain and in three somites in one embryo bearing each genotype. Nuclei stained brown strongly, lightly or partially (>50% of nucleus area) are characteristic of dividing cells and were counted as positive. Blue cells where only hematoxylin counterstaining was visible were considered negative.

TUNEL staining was performed as a measure of apoptosis with the *in situ* cell death detection kit, POD (Roche Diagnostics Corporation, IN), and used according to the manufacturer's instructions. Staining was visualized using 0.2 mg/ml diaminobenzadine (DAB) and 0.01% hydrogen peroxide in 0.1 M Tris, pH 7.2, as the peroxidase substrate. Counterstaining was performed with hematoxylin.

Photomicrographs of whole embryos and sections were taken through a Wild Heerbrugg dissecting microscope. Magnifications are indicated in respective Figure Legends.

Isolation of MEFs and doubling time

E8.5 embryos were obtained from *Mrad9b*$^{+/-}$ mouse inter-crosses and dissected from pregnant females. E13.5 embryos were obtained from *Mrad9b*$^{+/-}$x *Mrad9b*$^{+/+}$ matings. The procedure to isolate fibroblasts was as published (Joyner, 2000), with the exceptions that 1) E8.5 whole embryos were used, while head and internal organs were removed in E13.5 embryos, 2) glass beads were not used to disrupt the embryos, 3) trypsinization was for only 5–10 minutes, and 4) the cell culture dishes were coated with gelatin. Embryos were plated into 24 well dishes. When they reached confluency, fibroblasts that proliferated were replated into 6 wells first (first passage), followed by replating into 10 cm dishes (second passage). During passage of the cells, aliquots were used for determining genotype. For embryonic fibroblasts that did not proliferate, cell debris was used to determine genotype. To isolate DNA from the embryos and cells, the Direct PCR (yolk sac) kit from Viagen Biotech (Los Angeles, CA) was used. PCR primers and amplification conditions already described to assess the genotypes of adult mice were employed for the MEFs. The procedure used for calculating MEF doubling time was similar to the methods employed for determining the same characteristic of ES cells, as described above, but 10^5 MEFs were seeded in triplicate in gelatinized 6-well dishes to start. Cell numbers were determined every 24 hours. Doubling time was calculated in the exponential growth phase.

Cell survival assay

Mouse ES cells were seeded at low density in triplicate onto gelatinized six-well tissue culture dishes. Chemicals at indicated concentrations were added the next day. After 1 hr (mitomycin C and ethyl methanesulfonate), 2 hr (cisplatin) or 24 hr (hydroxyurea) exposure, cells were rinsed with PBS and fresh medium was added. Gamma irradiation (^{137}Cesium, dose rate of 0.86 Gy/min) was performed one day after plating. For all treatments, cells were fixed with 70% ethanol and stained with 2% gentian violet eight days after plating. Colonies were then counted. Percent survival was calculated as (number of colonies in treated dishes)/(number of colonies in untreated dishes) x 100.

Flow cytometry analysis

Exponentially growing cells were seeded (3×10^6 cells per 10 cm dish). Cells were irradiated 24 hr later with a dose of 8 Gy of gamma rays or mock treated. Some cells were also treated for 12 h with 12 µM nocodazole, which blocks cell cycle progression in G2. At various times after treatment, cells were harvested, washed twice in PBS, then fixed in 75% ethanol at 4°C for at least 4 hr and as long as overnight. Cells were washed once more in PBS and stained overnight at 4°C with propidium iodide solution (10 mM Tris-HCl pH 8, 0.7 mg/ml RNase A, 0.1% Nonidet P-40, 1 mM NaCl and 0.05 mg per ml propidium iodide), then analyzed using a FACSCalibur System (Becton Dickinson) and CellQuest software to assess cell cycle phase distribution of the populations. A minimum of 10,000 cells per each population were analyzed.

Sister chromatid exchange

Cells were grown for two cell division periods in medium containing 5 µM BrdU, pulsed with 0.5 µg/ml colcemid for two hours, harvested, resuspended in 0.56% KCl prewarmed at 37°C and incubated at 37°C for 10 min. Cells were then centrifuged to pellet, and fixed with methanol/acetic acid (3:1). This step was repeated 2 more times and cell preparations were stored overnight at 4°C. Cells were dropped onto slides and aged at room temperature for 1–3 days. Slides were incubated in 50 µg/ml Hoechst 33258 in PBS for 20 min and rinsed with PBS. Slides were covered with buffer (0.16 M sodium phosphate, 0.04 M sodium citrate, pH 7), a cover slip was then placed on top, sealed with rubber cement and exposed to UV black light for 30 min. Cover slips were removed and slides were washed in 2x SSC at 58°C for 5 min, dipped in 58°C water to remove salts, air dried and mounted with Vectashield containing DAPI (Vector Laboratories). Metaphase spreads were scanned at low magnification (x20) using Metafer 3 (Metasystems, Germany). Pictures (x100 magnification) of the metaphases were then taken under an Axioplan 2 Imaging Microscope equipped with a HBO 100 mercury lamp, a DAPI filter (Zeiss, Germany) and a CV-M300 charge-coupled device camera (Jai, CA). One hundred metaphase spreads per sample were analyzed using ISIS software (Metasystems).

Cytokinesis-block micronucleus assay

Exponentially growing cells were seeded into two chamber slides and treated with 6 µg/ml cytochalasin B for 24 h. Cytochalasin B blocks cytokinesis after one nuclear division, allowing accurate micronucleus scoring (Fenech, 2000). After cytochalasin B treatment, cells were fixed with 95% ethanol/ 5% acetic acid, rinsed three times with PBS and mounted with Vectashield containing DAPI (Vector Laboratories). A minimum of 500 binucleated cells for each population were scored for micronuclei.

Acknowledgments

We thank Ms. X. Wang for genotyping, Dr. A. Dutta for performing the M-FISH assay, Dr. T. Templin for statistical analysis, and Drs. A. Balajee, A. Bertucci, C. Geard, D. Warburton, and Ms. J. Nie for technical advice.

Grant Sponsors: National Institutes of Health. Grant numbers: CA130536, GM079107. Environmental Protection Agency: Research Training in Environmentally-Induced Cancers. Fellowship number: EPA-X972798.

REFERENCES

Budzowska M, Jaspers I, Essers J, de Waard H, van Drunen E, Hanada K, Beverloo B, Hendriks RW, de Klein A, Kanaar R, Hoeijmakers JH, Maas A. Mutation of the mouse Rad17 gene leads to embryonic lethality and reveals a role in DNA damage-dependent recombination. EMBO J. 2004; 23:3548–3558. [PubMed: 15297881]

Cang Y, Zhang J, Nicholas SA, Bastien J, Li B, Zhou P, Goff SP. Deletion of DDB1 in mouse brain and lens leads to p53-dependent elimination of proliferating cells. Cell. 2006; 127:929–940. [PubMed: 17129780]

Chapman DL, Wolgemuth DJ. Expression of proliferating cell nuclear antigen in the mouse germ line and surrounding somatic cells suggests both proliferation-dependent and -independent modes of function. Int J Dev Biol. 1994; 38:491–497. [PubMed: 7848832]

de Waard H, Sonneveld E, de Wit J, Esveldt-van Lange R, Hoeijmakers JH, Vrieling H, van der Horst GT. Cell-type-specific consequences of nucleotide excision repair deficiencies: Embryonic stem cells versus fibroblasts. DNA Repair (Amst). 2008; 7:1659–1669. [PubMed: 18634906]

Dianov GL, Parsons JL. Co-ordination of DNA single strand break repair. DNA Repair (Amst). 2007; 6:454–460. [PubMed: 17123872]

Dufault VM, Oestreich AJ, Vroman BT, Karnitz LM. Identification and characterization of RAD9B, a paralog of the RAD9 checkpoint gene. Genomics. 2003; 82:644–651. [PubMed: 14611806]

Fenech M. The in vitro micronucleus technique. Mutat Res. 2000; 455:81–95. [PubMed: 11113469]

Frank KM, Sekiguchi JM, Seidl KJ, Swat W, Rathbun GA, Cheng HL, Davidson L, Kangaloo L, Alt FW. Late embryonic lethality and impaired V(D)J recombination in mice lacking DNA ligase IV. Nature. 1998; 396:173–177. [PubMed: 9823897]

Friedberg EC, Meira LB. Database of mouse strains carrying targeted mutations in genes affecting biological responses to DNA damage Version 7. DNA Repair (Amst). 2006; 5:189–209. [PubMed: 16290067]

Fuertes MA, Alonso C, Perez JM. Biochemical modulation of Cisplatin mechanisms of action: enhancement of antitumor activity and circumvention of drug resistance. Chem Rev. 2003; 103:645–662. [PubMed: 12630848]

Gao Y, Sun Y, Frank KM, Dikkes P, Fujiwara Y, Seidl KJ, Sekiguchi JM, Rathbun GA, Swat W, Wang J, Bronson RT, Malynn BA, Bryans M, Zhu C, Chaudhuri J, Davidson L, Ferrini R, Stamato T, Orkin SH, Greenberg ME, Alt FW. A critical role for DNA end-joining proteins in both lymphogenesis and neurogenesis. Cell. 1998; 95:891–902. [PubMed: 9875844]

Gowen LC, Johnson BL, Latour AM, Sulik KK, Koller BH. Brca1 deficiency results in early embryonic lethality characterized by neuroepithelial abnormalities. Nat Genet. 1996; 12:191–194. [PubMed: 8563759]

Gu Y, Jin S, Gao Y, Weaver DT, Alt FW. Ku70-deficient embryonic stem cells have increased ionizing radiosensitivity, defective DNA end-binding activity, and inability to support V(D)J recombination. Proc Natl Acad Sci U S A. 1997; 94:8076–8081. [PubMed: 9223317]

Hakem R, de la Pompa JL, Sirard C, Mo R, Woo M, Hakem A, Wakeham A, Potter J, Reitmair A, Billia F, Firpo E, Hui CC, Roberts J, Rossant J, Mak TW. The tumor suppressor gene Brca1 is required for embryonic cellular proliferation in the mouse. Cell. 1996; 85:1009–1023. [PubMed: 8674108]

Hanawalt PC, Spivak G. Transcription-coupled DNA repair: two decades of progress and surprises. Nat Rev Mol Cell Biol. 2008; 9:958–970. [PubMed: 19023283]

Hanks MC, Loomis CA, Harris E, Tong CX, Anson-Cartwright L, Auerbach A, Joyner A. Drosophila engrailed can substitute for mouse Engrailed1 function in mid-hindbrain, but not limb development. Development. 1998; 125:4521–4530. [PubMed: 9778510]

Harris MJ, Juriloff DM. Mini-review: toward understanding mechanisms of genetic neural tube defects in mice. Teratology. 1999; 60:292–305. [PubMed: 10525207]

Helt CE, Wang W, Keng PC, Bambara RA. Evidence that DNA damage detection machinery participates in DNA repair. Cell Cycle. 2005; 4:529–532. [PubMed: 15876866]

Herrera RE, Sah VP, Williams BO, Makela TP, Weinberg RA, Jacks T. Altered cell cycle kinetics, gene expression, and G1 restriction point regulation in Rb-deficient fibroblasts. Mol Cell Biol. 1996; 16:2402–2407. [PubMed: 8628308]

Hogan B, BR.; Costantini, F.; Lacy, E. A laboratory Manual. Cold spring Harbor Laboratory Press; 1994. Manipulating the Mouse Embryo.

Hopkins KM, Auerbach W, Wang XY, Hande MP, Hang H, Wolgemuth DJ, Joyner AL, Lieberman HB. Deletion of mouse rad9 causes abnormal cellular responses to DNA damage, genomic instability, and embryonic lethality. Mol Cell Biol. 2004; 24:7235–7248. [PubMed: 15282322]

Hopkins KM, Wang X, Berlin A, Hang H, Thaker HM, Lieberman HB. Expression of mammalian paralogues of HRAD9 and Mrad9 checkpoint control genes in normal and cancerous testicular tissue. Cancer Res. 2003; 63:5291–5298. [PubMed: 14500360]

Hu Z, Liu Y, Zhang C, Zhao Y, He W, Han L, Yang L, Hopkins KM, Yang X, Lieberman HB, Hang H. Targeted deletion of Rad9 in mouse skin keratinocytes enhances genotoxin-induced tumor development. Cancer Res. 2008; 68:5552–5561. [PubMed: 18632607]

Jeggo P, Lobrich M. Radiation-induced DNA damage responses. Radiat Prot Dosimetry. 2006; 122:124–127. [PubMed: 17351270]

Johnston DS, Wright WW, Dicandeloro P, Wilson E, Kopf GS, Jelinsky SA. Stage-specific gene expression is a fundamental characteristic of rat spermatogenic cells and Sertoli cells. Proc Natl Acad Sci U S A. 2008; 105:8315–8320. [PubMed: 18544648]

Joyner, AL. Gene targeting: a practical approach. 2d ed.. New York, NY: IRL Press; 2000.

Kaufman, MH. The atlas of mouse development. Academic Press Limited; 1995.

Larminat F, Cambois G, Zdzienicka MZ, Defais M. Lack of correlation between repair of DNA interstrand cross-links and hypersensitivity of hamster cells towards mitomycin C and cisplatin. FEBS Lett. 1998; 437:97–100. [PubMed: 9804179]

Lieberman HB. Rad9, an evolutionarily conserved gene with multiple functions for preserving genomic integrity. J Cell Biochem. 2006; 97:690–697. [PubMed: 16365875]

Lim DS, Hasty P. A mutation in mouse rad51 results in an early embryonic lethal that is suppressed by a mutation in p53. Mol Cell Biol. 1996; 16:7133–7143. [PubMed: 8943369]

Liu CY, Flesken-Nikitin A, Li S, Zeng Y, Lee WH. Inactivation of the mouse Brca1 gene leads to failure in the morphogenesis of the egg cylinder in early postimplantation development. Genes Dev. 1996; 10:1835–1843. [PubMed: 8698242]

Liu Q, Guntuku S, Cui XS, Matsuoka S, Cortez D, Tamai K, Luo G, Carattini-Rivera S, DeMayo F, Bradley A, Donehower LA, Elledge SJ. Chk1 is an essential kinase that is regulated by Atr and required for the G(2)/M DNA damage checkpoint. Genes Dev. 2000; 14:1448–1459. [PubMed: 10859164]

Loeb LA, Harris CC. Advances in chemical carcinogenesis: a historical review and prospective. Cancer Res. 2008; 68:6863–6872. [PubMed: 18757397]

Ludwig T, Chapman DL, Papaioannou VE, Efstratiadis A. Targeted mutations of breast cancer susceptibility gene homologs in mice: lethal phenotypes of Brca1, Brca2, Brca1/Brca2, Brca1/p53, and Brca2/p53 nullizygous embryos. Genes Dev. 1997; 11:1226–1241. [PubMed: 9171368]

Luo G, Yao MS, Bender CF, Mills M, Bladl AR, Bradley A, Petrini JH. Disruption of mRad50 causes embryonic stem cell lethality, abnormal embryonic development, and sensitivity to ionizing radiation. Proc Natl Acad Sci U S A. 1999; 96:7376–7381. [PubMed: 10377422]

McHugh PJ, Spanswick VJ, Hartley JA. Repair of DNA interstrand crosslinks: molecular mechanisms and clinical relevance. Lancet Oncol. 2001; 2:483–490. [PubMed: 11905724]

Menon SG, Sarsour EH, Spitz DR, Higashikubo R, Sturm M, Zhang H, Goswami PC. Redox regulation of the G1 to S phase transition in the mouse embryo fibroblast cell cycle. Cancer Res. 2003; 63:2109–2117. [PubMed: 12727827]

Ng JM, Vrieling H, Sugasawa K, Ooms MP, Grootegoed JA, Vreeburg JT, Visser P, Beems RB, Gorgels TG, Hanaoka F, Hoeijmakers JH, van der Horst GT. Developmental defects and male sterility in mice lacking the ubiquitin-like DNA repair gene mHR23B. Mol Cell Biol. 2002; 22:1233–1245. [PubMed: 11809813]

Niida H, Nakanishi M. DNA damage checkpoints in mammals. Mutagenesis. 2006; 21:3–9. [PubMed: 16314342]

Nussenzweig A, Chen C, da Costa Soares V, Sanchez M, Sokol K, Nussenzweig MC, Li GC. Requirement for Ku80 in growth and immunoglobulin V(D)J recombination. Nature. 1996; 382:551–555. [PubMed: 8700231]

Orii KE, Lee Y, Kondo N, McKinnon PJ. Selective utilization of nonhomologous end-joining and homologous recombination DNA repair pathways during nervous system development. Proc Natl Acad Sci U S A. 2006; 103:10017–10022. [PubMed: 16777961]

Palom Y, Suresh Kumar G, Tang LQ, Paz MM, Musser SM, Rockwell S, Tomasz M. Relative toxicities of DNA cross-links and monoadducts: new insights from studies of decarbamoyl mitomycin C and mitomycin C. Chem Res Toxicol. 2002; 15:1398–1406. [PubMed: 12437330]

Pandita RK, Sharma GG, Laszlo A, Hopkins KM, Davey S, Chakhparonian M, Gupta A, Wellinger RJ, Zhang J, Powell SN, Roti Roti JL, Lieberman HB, Pandita TK. Mammalian Rad9 plays a role in telomere stability, S- and G2-phase-specific cell survival, and homologous recombinational repair. Mol Cell Biol. 2006; 26:1850–1864. [PubMed: 16479004]

Pietenpol JA, Stewart ZA. Cell cycle checkpoint signaling: cell cycle arrest versus apoptosis. Toxicology. 2002; 181–182:475–481.

Rabik CA, Dolan ME. Molecular mechanisms of resistance and toxicity associated with platinating agents. Cancer Treat Rev. 2007; 33:9–23. [PubMed: 17084534]

Robertson AB, Klungland A, Rognes T, Leiros I. Base excision repair: the long and short of it. Cell Mol Life Sci. 2009; 66:981–983. [PubMed: 19153658]

Sah VP, Attardi LD, Mulligan GJ, Williams BO, Bronson RT, Jacks T. A subset of p53-deficient embryos exhibit exencephaly. Nat Genet. 1995; 10:175–180. [PubMed: 7663512]

Sega GA. A review of the genetic effects of ethyl methanesulfonate. Mutat Res. 1984; 134:113–142. [PubMed: 6390190]

Sharan SK, Morimatsu M, Albrecht U, Lim DS, Regel E, Dinh C, Sands A, Eichele G, Hasty P, Bradley A. Embryonic lethality and radiation hypersensitivity mediated by Rad51 in mice lacking Brca2. Nature. 1997; 386:804–810. [PubMed: 9126738]

Sobol RW, Horton JK, Kuhn R, Gu H, Singhal RK, Prasad R, Rajewsky K, Wilson SH. Requirement of mammalian DNA polymerase-beta in base-excision repair. Nature. 1996; 379:183–186. [PubMed: 8538772]

Suzuki A, de la Pompa JL, Hakem R, Elia A, Yoshida R, Mo R, Nishina H, Chuang T, Wakeham A, Itie A, Koo W, Billia P, Ho A, Fukumoto M, Hui CC, Mak TW. Brca2 is required for embryonic cellular proliferation in the mouse. Genes Dev. 1997; 11:1242–1252. [PubMed: 9171369]

Tebbs RS, Flannery ML, Meneses JJ, Hartmann A, Tucker JD, Thompson LH, Cleaver JE, Pedersen RA. Requirement for the Xrcc1 DNA base excision repair gene during early mouse development. Dev Biol. 1999; 208:513–529. [PubMed: 10191063]

Warren AJ, Ihnat MA, Ogdon SE, Rowell EE, Hamilton JW. Binding of nuclear proteins associated with mammalian DNA repair to the mitomycin C-DNA interstrand crosslink. Environ Mol Mutagen. 1998; 31:70–81. [PubMed: 9464318]

Weiss RS, Enoch T, Leder P. Inactivation of mouse Hus1 results in genomic instability and impaired responses to genotoxic stress. Genes Dev. 2000; 14:1886–1898. [PubMed: 10921903]

Xiao Y, Weaver DT. Conditional gene targeted deletion by Cre recombinase demonstrates the requirement for the double-strand break repair Mre11 protein in murine embryonic stem cells. Nucleic Acids Res. 1997; 25:2985–2991. [PubMed: 9224597]

Yin Y, Zhu A, Jin YJ, Liu YX, Zhang X, Hopkins KM, Lieberman HB. Human RAD9 checkpoint control/proapoptotic protein can activate transcription of p21. Proc Natl Acad Sci U S A. 2004; 101:8864–8869. [PubMed: 15184659]

Zha S, Alt FW, Cheng HL, Brush JW, Li G. Defective DNA repair and increased genomic instability in Cernunnos-XLF-deficient murine ES cells. Proc Natl Acad Sci U S A. 2007; 104:4518–4523. [PubMed: 17360556]

Zhong Q, Boyer TG, Chen PL, Lee WH. Deficient nonhomologous end-joining activity in cell-free extracts from Brca1-null fibroblasts. Cancer Res. 2002; 62:3966–3970. [PubMed: 12124328]

Zhu A, Zhang CX, Lieberman HB. Rad9 has a functional role in human prostate carcinogenesis. Cancer Res. 2008; 68:1267–1274. [PubMed: 18316588]

Zhu J, Petersen S, Tessarollo L, Nussenzweig A. Targeted disruption of the Nijmegen breakage syndrome gene NBS1 leads to early embryonic lethality in mice. Curr Biol. 2001; 11:105–109. [PubMed: 11231126]

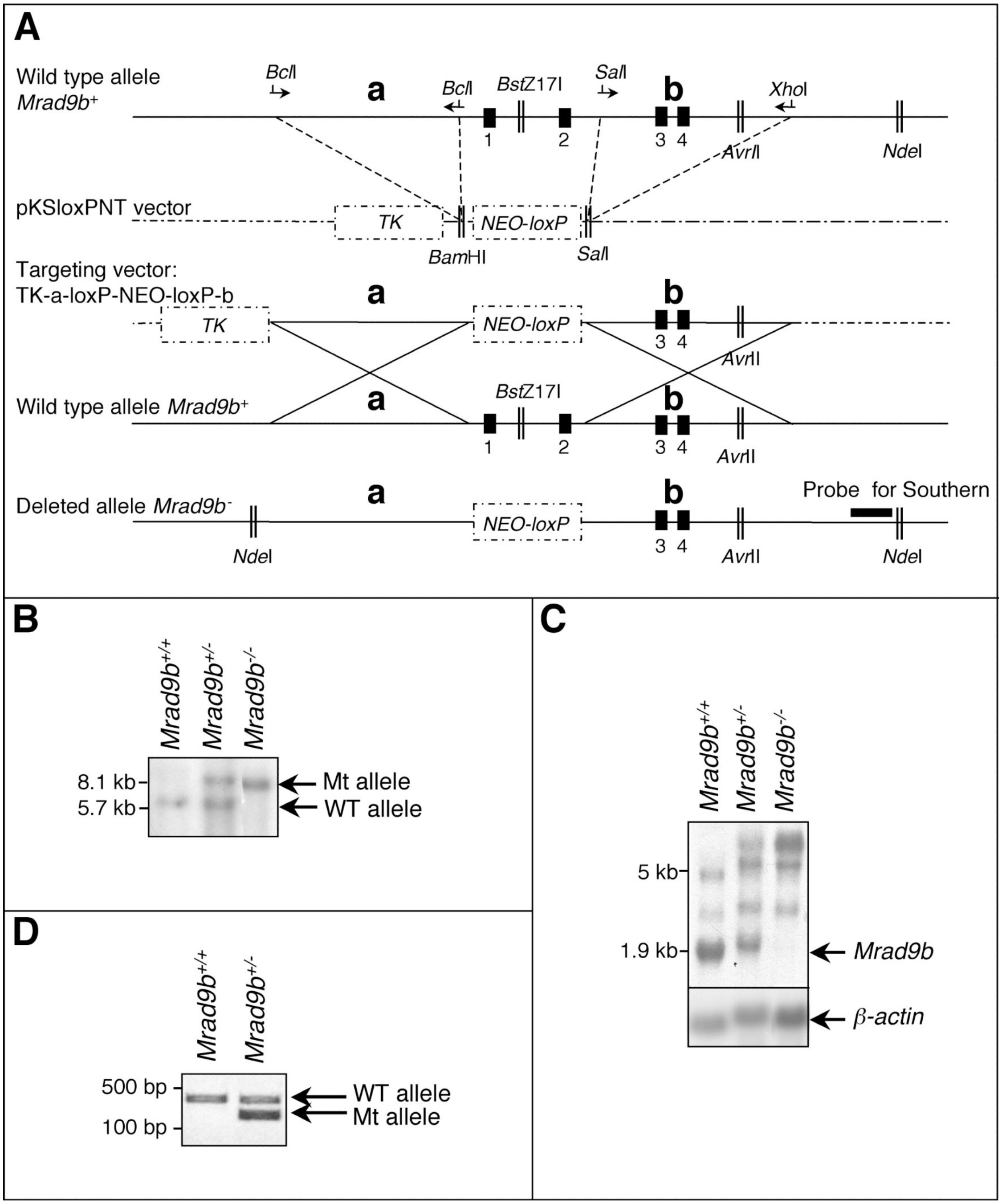

Figure 1.

(A) Targeted disruption of the mouse *Mrad9b* gene. Vector-derived sequences are shown as stippled lines; genomic DNA illustrated as continuous lines. Arrows represent primers for PCR amplification; Vertical black boxes (1–4) are the first four exons of *Mrad9b*. *NEO*, neomycin resistance gene. *TK*, thymidine kinase. **a** and **b** are two *Mrad9b* genomic fragments that were amplified by PCR, ligated into pKSloxPNT vector and used for homologous recombination between the targeting construct and the corresponding genomic region. Areas of homology are depicted by large "Xs". The targeting vector was linearized with *Avr*II before transfection into ES cells. **(B)** Southern blot analysis of *Mrad9b* in *Mrad9b*$^{+/+}$, *Mrad9b*$^{+/-}$ (clone #341) and *Mrad9b*$^{-/-}$ mouse ES cells. The pattern for

Mrad9b$^{+/-}$ (clone #350) was the same as for clone #341 (data not shown). Genomic DNA was digested with *Nde*I and *Bst*Z17I, separated on an agarose gel, and probed. **(C)** Northern blot analysis of *Mrad9b* expression in *Mrad9b*$^{+/+}$*Mrad9b*$^{+/-}$ (clone #341) and *Mrad9b*$^{-/-}$ mouse ES cells. Expression in *Mrad9b*$^{+/-}$ ES cell clone #350 (data not shown) was similar to that in clone #341. Beta–actin served as the internal control. **(D)** Genotyping of mice by PCR using tail DNA. WT, wild type; Mt, deletion mutant.

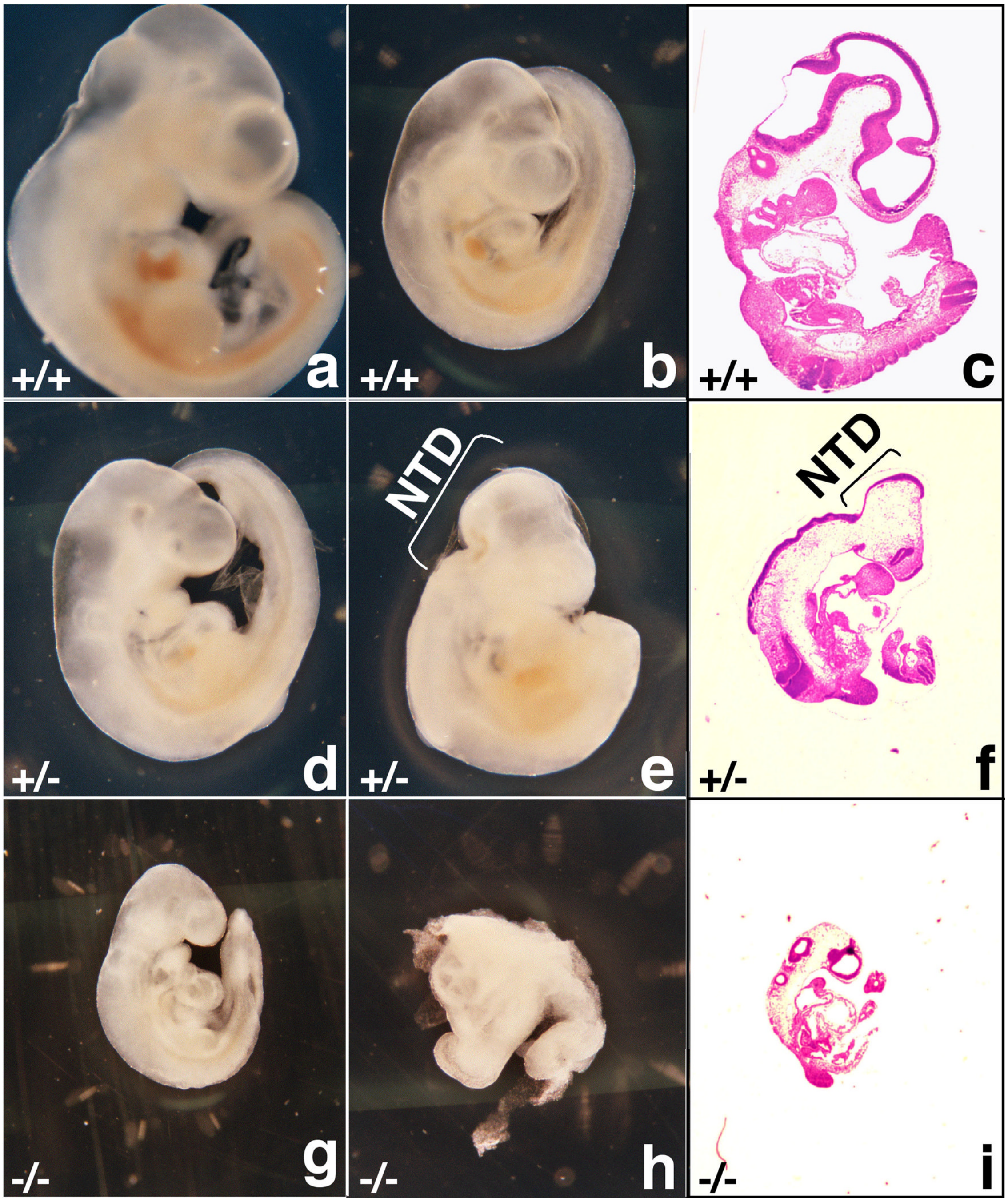

Figure 2.

Morphology (a, b, d, e, g, h) and histological sections (c, f, i) of E10.5 mouse embryos derived from a *Mrad9b*$^{+/-}$ x *Mrad9b*$^{+/-}$ mating. All embryos are from the same litter. (a, c) and (b) *Mrad9b*$^{+/+}$ embryos displaying normal gross morphology but of different size. (d) *Mrad9b*$^{+/-}$ embryo displaying normal gross morphology, (e, f) *Mrad9b*$^{+/-}$ embryo displaying a defect in neural tube closure. (g, i) *Mrad9b*$^{-/-}$ embryo growth arrested, (h) *Mrad9b*$^{-/-}$ embryo resorbed. NTD: neural tube defect.

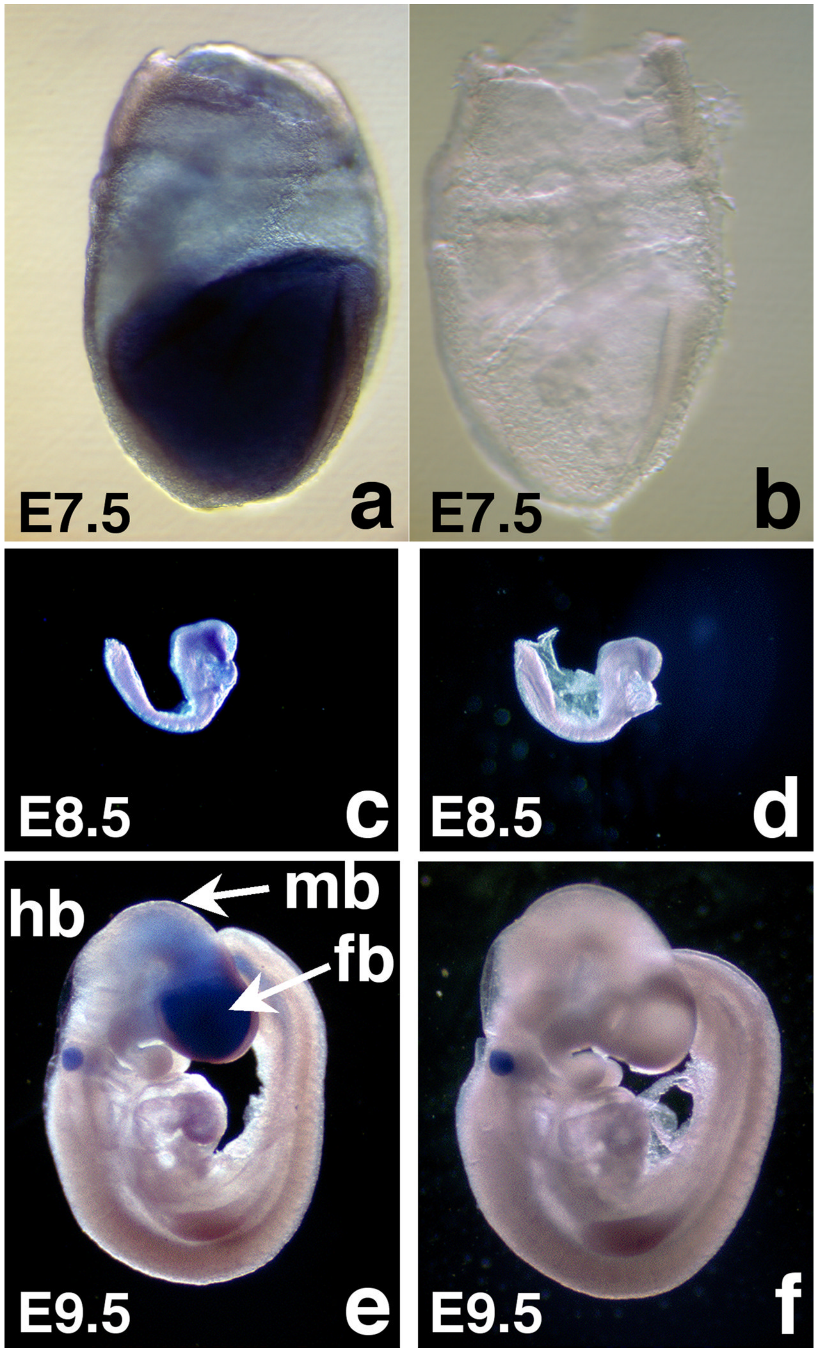

Figure 3.

Whole mount *in situ* hybridization of *Mrad9b*$^{+/+}$ mouse embryos probed with *Mrad9b* sense (a, c, e) and antisense (b, d, f) probes. (a, b) E7.5 embryos (×10 magnification), (c, d) E8.5 embryos (×2 magnification), (e, f) E9.5 embryos (×2 magnification). fb: forebrain, hb: hindbrain, mb: midbrain.

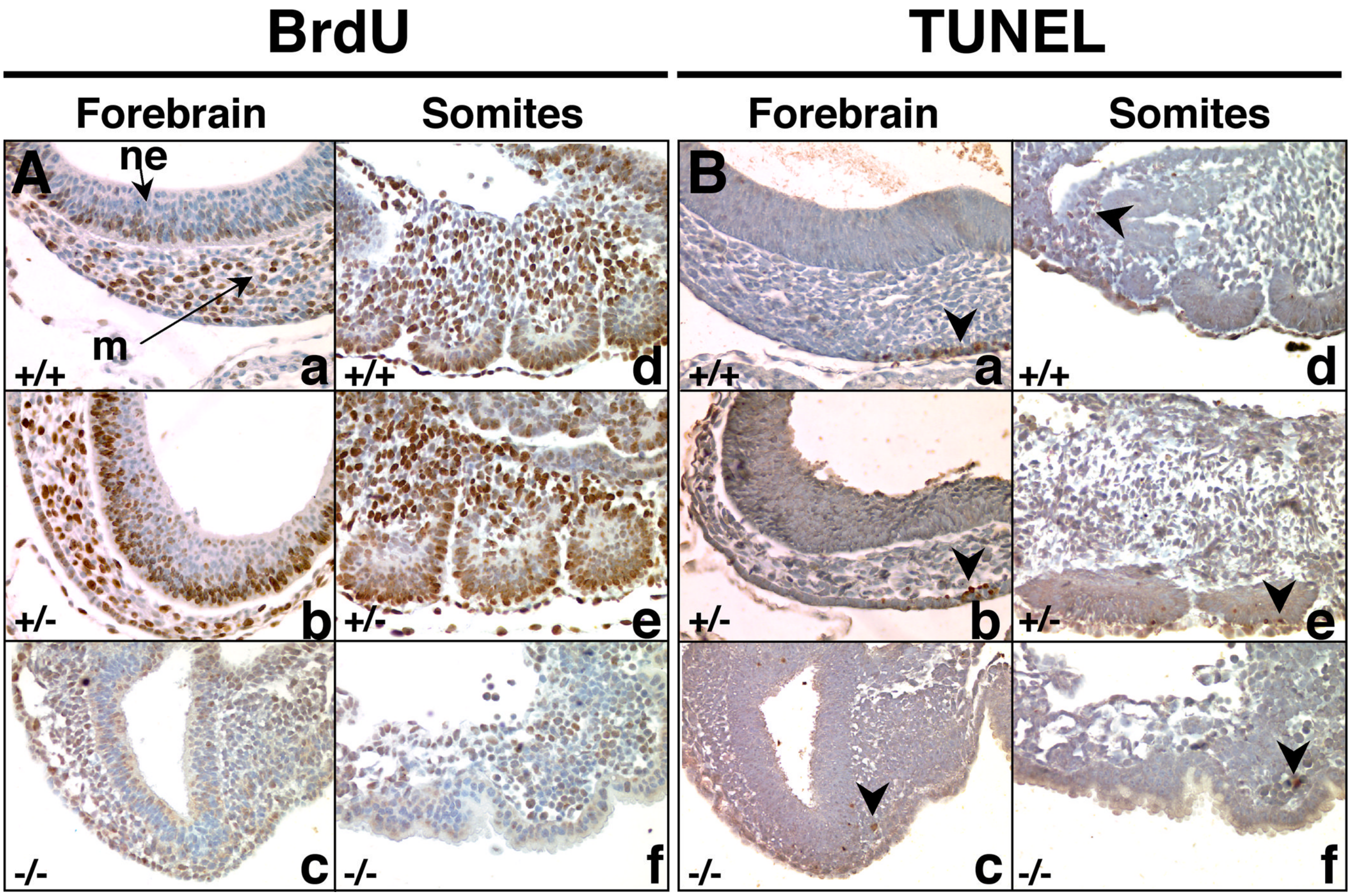

Figure 4.

(A) BrdU uptake in E9.5 embryos as a measure of cell proliferation. Nuclei that incorporated BrdU are stained brown. **(B)** TUNEL staining in E9.5 embryos to detect apoptosis. Exposed DNA ends characteristic of apoptotic cells were labeled brown. In both A and B sets of pictures, (a, b, c) represent the forebrain and (d, e, f) represent somites. +/+ indicates *Mrad9b*$^{+/+}$; +/− indicates *Mrad9b*$^{+/-}$; −/− indicates *Mrad9b*$^{-/-}$. The three embryos are from the same litter. m: mesenchyme, ne: neural epithelium. Arrowhead indicates apoptotic cell(s). Magnification ×40.

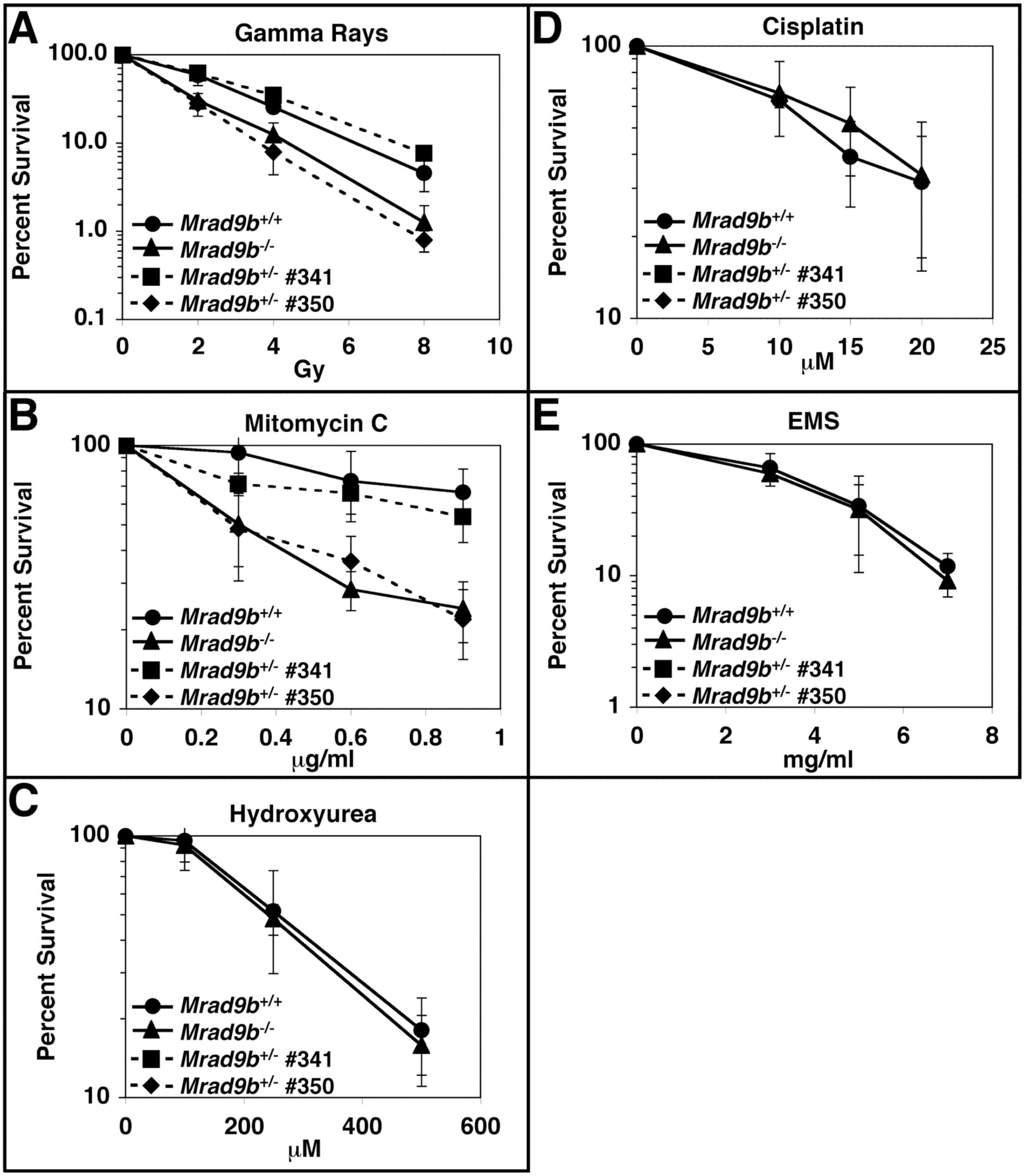

Figure 5.

Sensitivity of *Mrad9b*$^{+/+}$, *Mrad9b*$^{+/-}$ and *Mrad9b*$^{-/-}$ mouse ES cells to DNA damaging agents. Continuous lines, closed circles, *Mrad9b*$^{+/+}$ ES cells; Continuous lines, closed triangles, *Mrad9b*$^{-/-}$ ES cells; Dashed lines, closed squares, *Mrad9b*$^{+/-}$ ES cells #341; Dashed lines, closed diamonds, *Mrad9b*$^{+/-}$ ES cells #350. **(A)** Gamma rays; **(B)** Mitomycin C; **(C)** Hydroxyurea; **(D)** Cisplatin; **(E)** Ethyl methanesulfonate (EMS). Points are the mean of three to four experiments. Error bars indicate standard deviation.

NIH-PA Author Manuscript
NIH-PA Author Manuscript

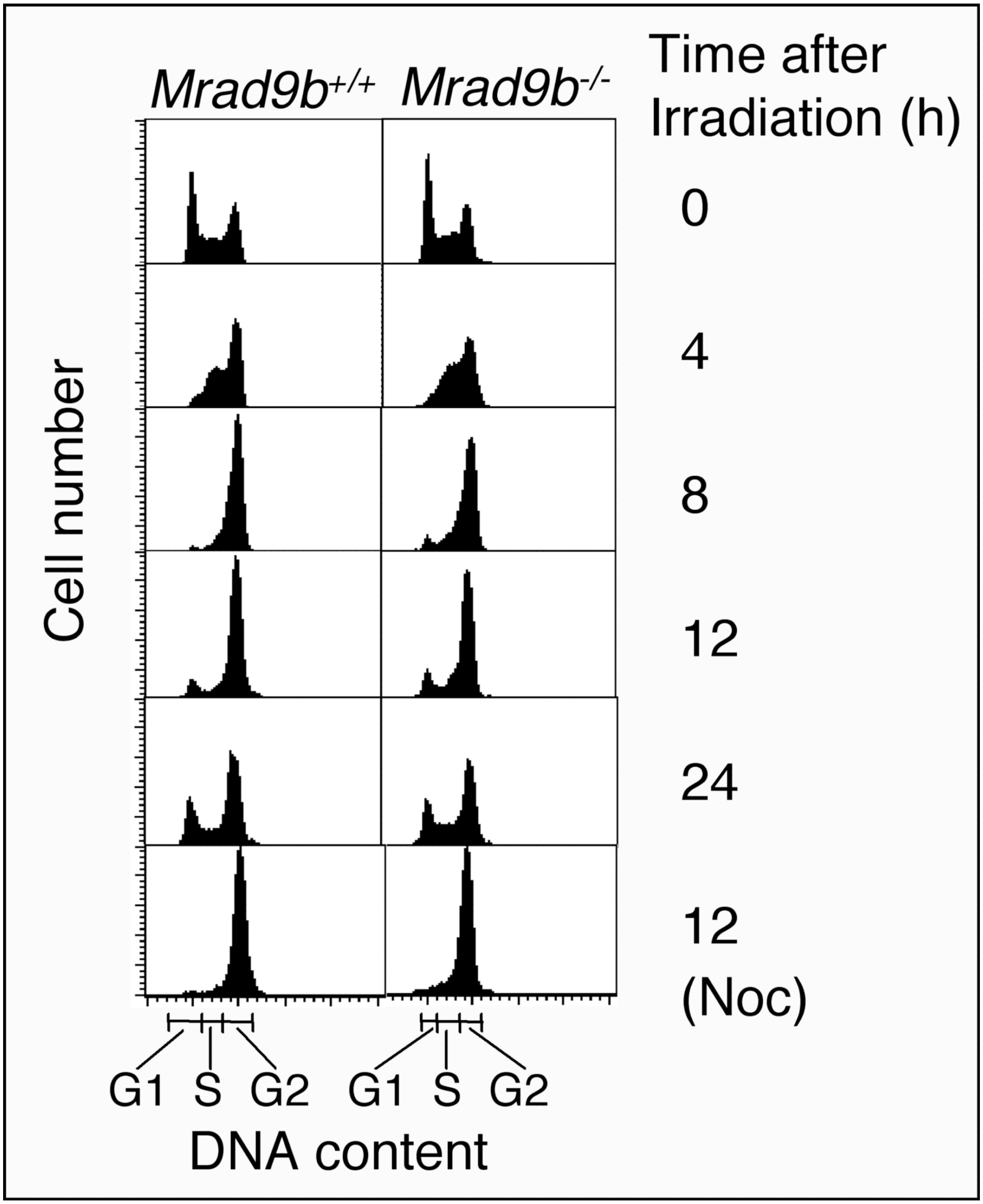

Figure 6.

Flow cytometric analysis of *Mrad9b*$^{+/+}$ and *Mrad9b*$^{-/-}$ ES cells mock treated or exposed to a dose of 8 Gy of gamma rays in the absence or presence of nocodazole (Noc). The 0 h point corresponds to unirradiated cells.

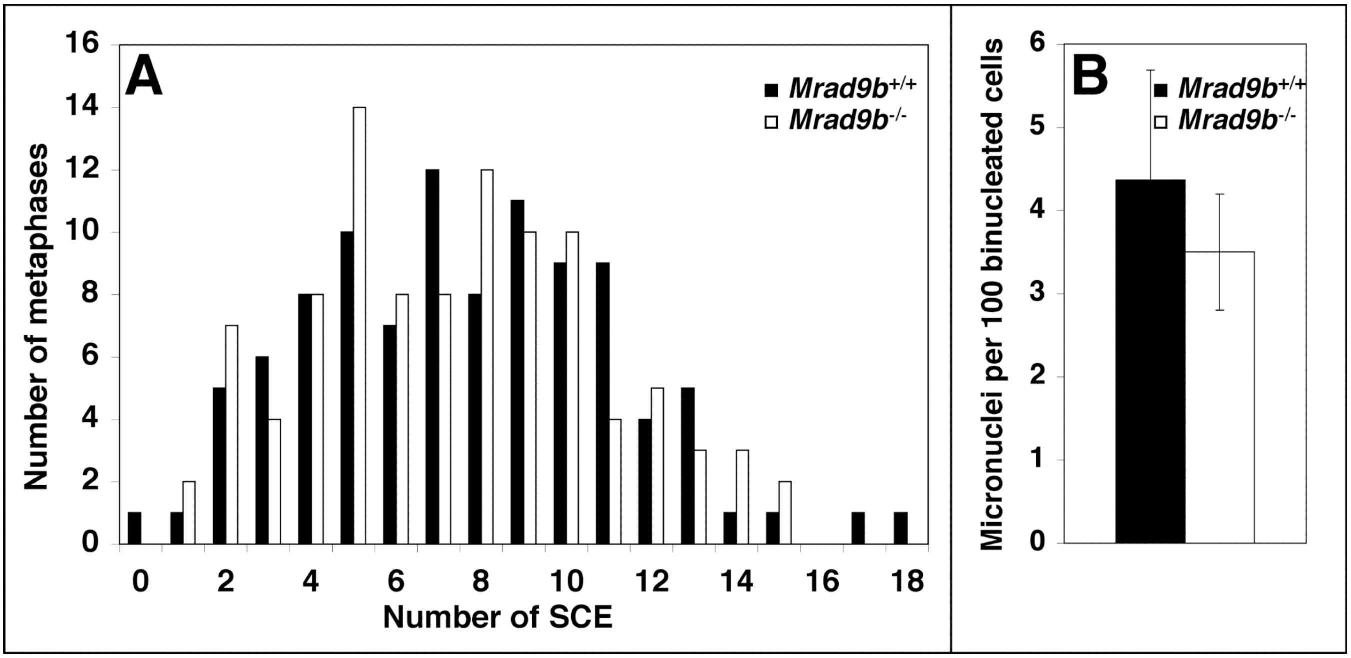

Figure 7.

Genomic stability of *Mrad9b*$^{+/+}$ and *Mrad9b*$^{-/-}$ ES cells. **(A)** Spontaneous sister chromatid exchange (SCE) in *Mrad9b*$^{+/+}$ (black columns) and *Mrad9b*$^{-/-}$ (white columns) ES cells. The spread of numbers of SCEs per given number of metaphases in *Mrad9b*$^{+/+}$ versus *Mrad9b*$^{-/-}$ ES cells is not significantly different as calculated by the F-test for homogeneity of variance (p=0.6). **(B)** Spontaneous micronuclei formation in *Mrad9b*$^{+/+}$ (black bar) and *Mrad9b*$^{-/-}$ ES cells (white bar). Cell division was blocked after one cycle with cytochalasin B and micronuclei were scored. Data are the mean of three experiments. Bars indicate standard deviation. There is no significant difference between the number of micronuclei in *Mrad9b*$^{+/+}$ versus *Mrad9b*$^{-/-}$ cells as calculated by the Student's t-test (p=0.4).

Table 1

Genotypes of mouse embryos and progeny derived from timed *Mrad9b*$^{+/-}$ x *Mrad9b*$^{+/-}$ matings.

Stage (Day)	Number of Embryos with Indicated Genotypes		
	Mrad9b$^{+/+}$	***Mrad9b***$^{+/-}$	***Mrad9b***$^{-/-}$
E7.5	3	6	10
E8.5	16 (1 resorbed)	32 (1 resorbed)	13 (3 resorbed)
E9.5	9	21	10 (10 resorbed)
E10.5	9	16	6 (5 resorbed)
E11.5	6	13	0
E12.5	6	13	0
E14.5	11	13	0
4 weeks postnatally	43	38	0

Table 2

Somite number as a function of *Mrad9b* genotype in E8.5 embryos.

Number of Somites	Number of Embryos with Indicated Number of Somites		
	Mrad9b$^{+/+}$	*Mrad9b*$^{+/-}$	*Mrad9b*$^{-/-}$
0		1	
1			
2			
3		3	
4			
5	1		
6	2	1	
7	1		1
8	2	2	
9	1	1	
10		1	
11		1	

Table 3

Percentage of cells at different phases of the cell cycle either mock-treated or at different times after exposure to 8 Gy of gamma rays.

Genotype	Time (h) Postirradiation	% of Population in Cell Cycle Phase*		
		G1	S	G2/M
Mrad9b$^{+/+}$	0	35.1±4.01	28.5±6.15	36.4±2.14
	4	6.8±3.15	37.4±4.44	55.8±1.29
	8	3.8±0.32	13.8±4.14	82.4±4.46
	12	9.2±0.67	9.9±2.52	80.9±3.19
	24	21.1±4.26	16.8±3.85	62.0±0.42
	12 + Noc	0.7±0.23	2.5±0.31	96.9±0.54
Mrad9b$^{-/-}$	0	30.8±5.60	32.5±5.99	36.7±11.59
	4	5.7±1.70	39.4±5.24	54.9±3.54
	8	2.6±3.00	17.5±1.67	79.9±4.67
	12	7.4±3.13	12.4±4.55	80.1±7.68
	24	14.7±7.31	20.8±6.97	64.5±14.28
	12 + Noc	1.1±0.67	5.6±1.22	93.3±1.89

*Data represent the mean of two experiments ± standard deviation.